AGU ADVANCING EARTH AND SPACE SCIENCE

Geophysical Research Letters®

RESEARCH LETTER
10.1029/2022GL098773

The Overlooked Role of the Stratosphere Under a Solar Constant Reduction

Ewa M. Bednarz[1], Daniele Visioni[1], Antara Banerjee[2,3], Peter Braesicke[4], Ben Kravitz[5,6], and Douglas G. MacMartin[1]

[1]Sibley School of Mechanical and Aerospace Engineering, Cornell University, Ithaca, NY, USA, [2]Cooperative Institute for Research in Environmental Sciences, University of Colorado Boulder, Boulder, CO, USA, [3]National Oceanic and Atmospheric Administration, Chemical Sciences Laboratory, Boulder, CO, USA, [4]IMK-ASF, Karlsruhe Institute of Technology, Eggenstein-Leopoldshafen, Germany, [5]Department of Earth and Atmospheric Sciences, Indiana University, Bloomington, IN, USA, [6]Atmospheric Sciences and Global Change Division, Pacific Northwest National Laboratory, Richland, WA, USA

Abstract Modeling experiments reducing surface temperatures via an idealized reduction of the solar constant have often been used as analogs for Stratospheric Aerosol Injection (SAI), thereby implicitly assuming that solar dimming captures the essential physical mechanism through which SAI influences surface climate. While the omission of some important processes that otherwise operate under SAI was identified before, here we demonstrate that the imposed reduction in the incoming solar radiation also induces a different stratospheric dynamical response, manifested through a weakening of the polar vortex, that propagates from the upper stratosphere down to the troposphere. The coupled stratospheric-tropospheric response exerts a previously overlooked first-order influence on southern hemispheric surface climate in the solar dimming experiments, including on the position of the tropospheric jet and Hadley Circulation and thus, ultimately, precipitation patterns. This perturbation, opposite to that expected under SAI, highlights the need for caution when attributing responses in idealized experiments.

Plain Language Summary Adverse impacts of climate change have pushed research on temperature reduction strategies like geoengineering into the spotlight. Possible impacts of geoengineering have long been assessed using "solar dimming" climate model experiments, which reduce surface temperatures via an idealized reduction of the incoming solar radiation as an analogue for injecting sulfate aerosols into the lower stratosphere (Stratospheric Aerosol Injection, SAI). We demonstrate that solar dimming induces previously overlooked circulation changes in the stratosphere that propagate down to the troposphere and exert a first-order influence on the Southern Hemisphere surface climate. This allows for an erroneous attribution of the simulated surface responses to the impacts of SAI geoengineering. The results also emphasize the importance of the stratosphere as an active contributor to the Southern Hemisphere near-surface climate change, and have implications for paleoclimate studies.

Key Points:

- Solar dimming induces previously overlooked stratospheric dynamical response
- The coupled stratospheric-tropospheric response exerts a first-order influence on the Southern Hemisphere (SH) surface climate in the solar dimming experiments
- The results emphasize the importance of the stratosphere, as well as the troposphere, as an active contributor to the SH climate change

Supporting Information:

Supporting Information may be found in the online version of this article.

Correspondence to:

E. M. Bednarz,
ewa.bednarz@cornell.edu

Citation:

Bednarz, E. M., Visioni, D., Banerjee, A., Braesicke, P., Kravitz, B., & MacMartin, D. G. (2022). The overlooked role of the stratosphere under a solar constant reduction. *Geophysical Research Letters*, *49*, e2022GL098773. https://doi.org/10.1029/2022GL098773

Received 19 MAR 2022
Accepted 7 JUN 2022

Author Contributions:

Conceptualization: Ewa M. Bednarz
Data curation: Daniele Visioni
Formal analysis: Ewa M. Bednarz
Funding acquisition: Douglas G. MacMartin
Methodology: Ewa M. Bednarz, Daniele Visioni, Antara Banerjee
Validation: Peter Braesicke
Visualization: Ewa M. Bednarz
Writing – original draft: Ewa M. Bednarz, Daniele Visioni
Writing – review & editing: Ewa M. Bednarz, Daniele Visioni, Antara Banerjee, Peter Braesicke, Ben Kravitz, Douglas G. MacMartin

1. Introduction

The potential overshoot in the near future of surface temperature thresholds deemed "safe" by international accords like the Paris Agreement has pushed research on temporary temperature reduction strategies like geoengineering into the spotlight. Climate intervention methods that reduce the incoming solar radiation have been proposed, when applied in conjunction with substantial cuts in greenhouse gas emissions, to offset some of the negative impacts of the present-day and future climate change (NASEM, 2021). The injection of sulfate aerosol precursors into the stratosphere (Stratospheric Aerosol Injection, SAI) has been given particular attention, in part due to it having a natural analogue in the form of explosive volcanic eruptions (Crutzen, 2006). Earth System Models have been considered an invaluable tool for assessing the feasibility, efficacy, and climatic impacts of such an approach. A detailed simulation of aerosol microphysics and its interactions with atmospheric radiation, chemistry, and dynamics under hypothetical SAI requires significant climate model complexity and computational expense; it is also reliant on parametrizations of aerosol microphysics in which large uncertainties exist (Visioni, MacMartin, Kravitz, et al., 2021). Therefore, simpler experiments have been previously used to study potential first-order climate impacts from SAI where the reduction of the incoming shortwave radiation

and, hence, surface temperatures is achieved by reducing the value of the solar constant in the models (e.g., Govindasamy & Caldeira, 2000; Kravitz et al., 2013).

However, multiple studies showed that in several respects reducing the solar constant is not representative of atmospheric impacts from geoengineering using SAI. Namely, solar dimming simulations do not include the aerosol-driven warming of the tropical lower stratosphere and its impacts on stratospheric and tropospheric circulation (Ferraro et al., 2015; McCusker et al., 2015; Simpson et al., 2019; Visioni et al., 2020), nor accelerated heterogeneous lower stratospheric ozone depletion (Tilmes et al., 2008), nor the increase in the ratio between the scattered to direct shortwave radiation in the troposphere (Kalidindi et al., 2015; Visioni, MacMartin, & Kravitz, 2021; Xia et al., 2017).

However, while the SAI-induced changes in stratospheric dynamics have been identified before, possible changes in stratospheric circulation directly induced by the reduction in solar constant have not, however, so far been recognized in this context as being relevant for the surface response. Yet, the importance of stratospheric variability for surface climate has been recognized in other contexts, for instance regarding the 11-year solar cycle. In that case, fluctuations in the incoming shortwave radiation and subsequent heating of the upper stratosphere initiate a stratospheric dynamical response in the high latitudes that can propagate down to the troposphere via positive feedbacks with planetary waves; this process can thus play an important role in modulating decadal surface climate variability (e.g., Kodera & Kuroda, 2002; Gray et al., 2010; Thiéblemont et al., 2015). Additionally, the cooling of the Antarctic springtime lower stratosphere caused by the substantial ozone depletion has been shown to have driven a stratospheric dynamical response that significantly impacted the Southern Hemisphere (SH) tropospheric climate over the second part of the 21st century (Banerjee et al., 2020; McLandress et al., 2011; Polvani et al., 2011; Son et al., 2009). Here, we posit that stratospheric circulation changes also play an important role under solar dimming. Indeed, we demonstrate previously unacknowledged impacts on the SH surface climate, making solar dimming a poor analogue for SAI geoengineering.

2. Methods

2.1. CESM Simulations

We use two sets of simulations performed using the Community Earth System Model with the Whole Atmosphere Community Climate Model (CESM1-WACCM, Mills, et al., 2017), a state-of-the-art climate model run with the horizontal resolution of $0.9° \times 1.25°$ and 70 vertical levels up to ∼140 km. The detailed description of these model simulations can be found in Visioni, MacMartin, and Kravitz (2021) and Kravitz et al. (2019) but we describe them briefly here. Both sets of experiments consist of three independent ensemble members each and are run under the RCP8.5 emission scenario, where the period 2070–2089 is analyzed. In the first experiment (CESMsolar), the total solar irradiance is reduced to maintain the global mean surface temperature at the 2010–2030 levels. In the second experiment (CESMsulfur), the global mean surface temperature is maintained at the 2010–2030 levels by means of SO_2 injection at the equator at approx. 25 km in altitude. The experiments are compared against the analogous four-member ensemble of CESM1 simulations carried out under RCP8.5 emissions but without geoengineering, as described in Tilmes et al. (2018).

2.2. GeoMIP Simulations

We use multi-model simulations carried out as part of the Geoengineering Model Intercomparison Project (GeoMIP, Kravitz et al., 2015), which itself constitutes part of the Phase 6 Climate Model Intercomparison Project (CMIP6, Eyring et al., 2016). In particular, we analyze the results of two geoengineering experiments, G6sulfur and G6solar. These experiments aim to the offset radiative forcing from increasing greenhouse gases following the Shared Socioeconomic Pathway 5–8.5 (SSP5-8.5, Meinshausen et al., 2020) by means of either injecting SO_2 between 10°N and 10°S at 20 km (G6sulfur) or by reducing the global mean solar constant (G6solar). This aims to produce similar global mean surface temperatures as corresponding simulations following the SSP2-4.5 pathway. Further details of the simulations, including more information on the participating models and the number of simulations performed by each can be found in Visioni, MacMartin, Kravitz, et al. (2021).

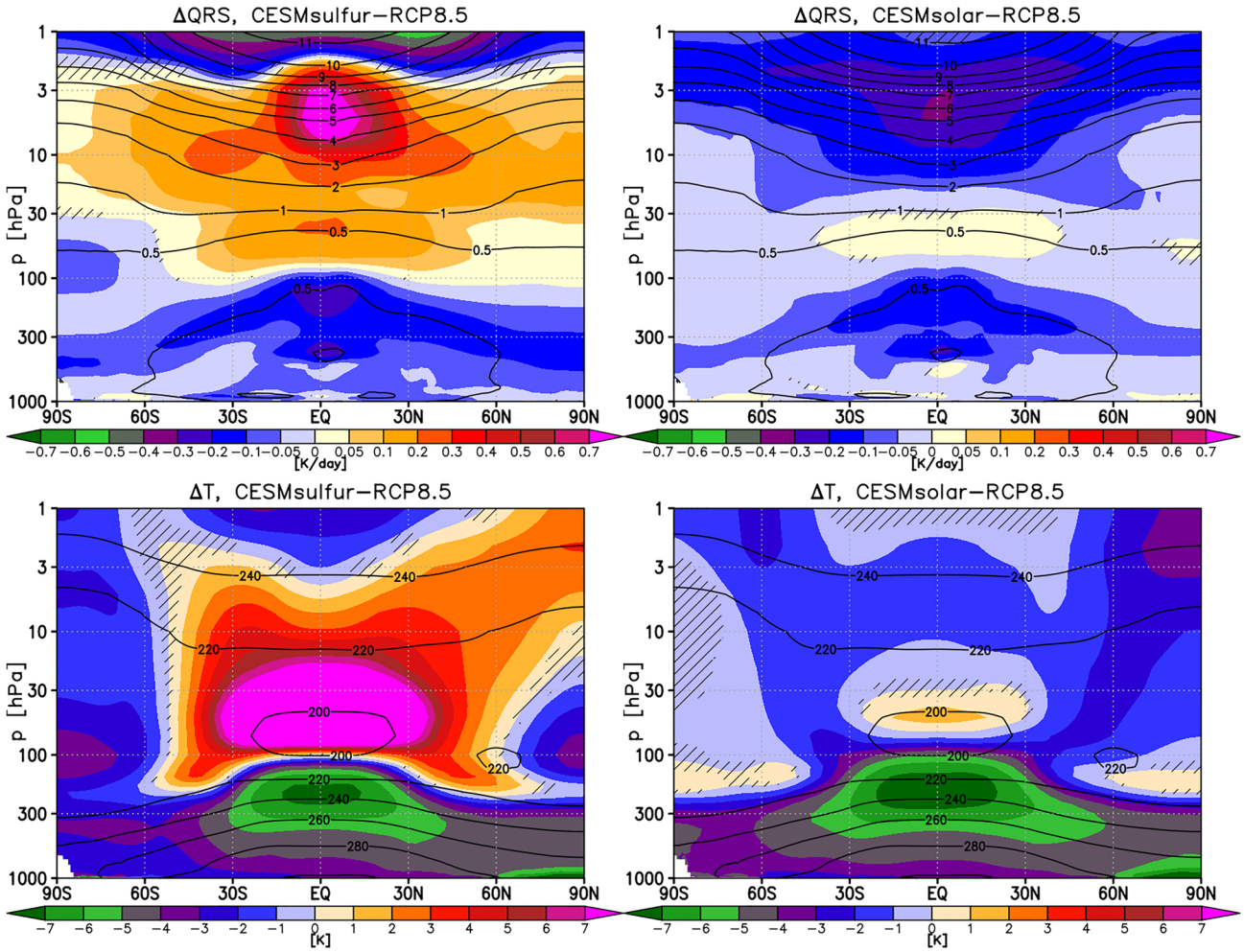

Figure 1. Radiative and temperature response to Stratospheric Aerosol Injection and solar dimming. Shading: Annual mean differences in (top) short wave heating rates (K day^{-1}) and (bottom) in temperature (K), averaged over 2070–2089, between CESMsulfur and RCP8.5 experiments (left), and between CESMsolar and RCP8.5 experiments (right). Hatching indicates regions where the difference is not statistically significant (±2 standard errors). Contours show the RCP8.5 climatology for reference.

3. Stratospheric Response to Solar Dimming versus SAI

First, we discuss the stratospheric response to solar dimming simulated in CESM1-WACCM Earth System Model. We use a set of simulations, henceforth labeled CESMsolar, where the incoming solar radiation is reduced in order to offset the increase in global mean surface temperature under the RCP8.5 GHG scenario to the present-day level. We compare these to analogous simulations where the reduction in surface temperature to present-day levels is achieved by the means of injecting sulfate aerosol precursors into the equatorial lower stratosphere, henceforth labeled CESMsulfur.

Both CESMsolar and CESMsulfur show reduced tropospheric temperatures relative to RCP8.5, consistent with the reduction in the absorption of incoming shortwave radiation (Figure 1). The tropospheric temperature responses are broadly similar in the two experiments, illustrating that solar dimming successfully simulates the direct radiative impact of SAI on the tropospheric climate. In the stratosphere, however, the absorption of solar and terrestrial radiation by sulfate aerosols in CESMsulfur (Figure S1 in Supporting Information S1) leads to a significant warming in the tropics, as evidenced by the increase in shortwave heating rates simulated over most of the stratosphere. We note that the simulated stratospheric temperature changes reflect a combination of changes in both the short- and longwave heating rates as well as any indirect dynamical changes; all of these would also be modulated by the associated changes in stratospheric ozone (Figure S2 in Supporting Information S1). We

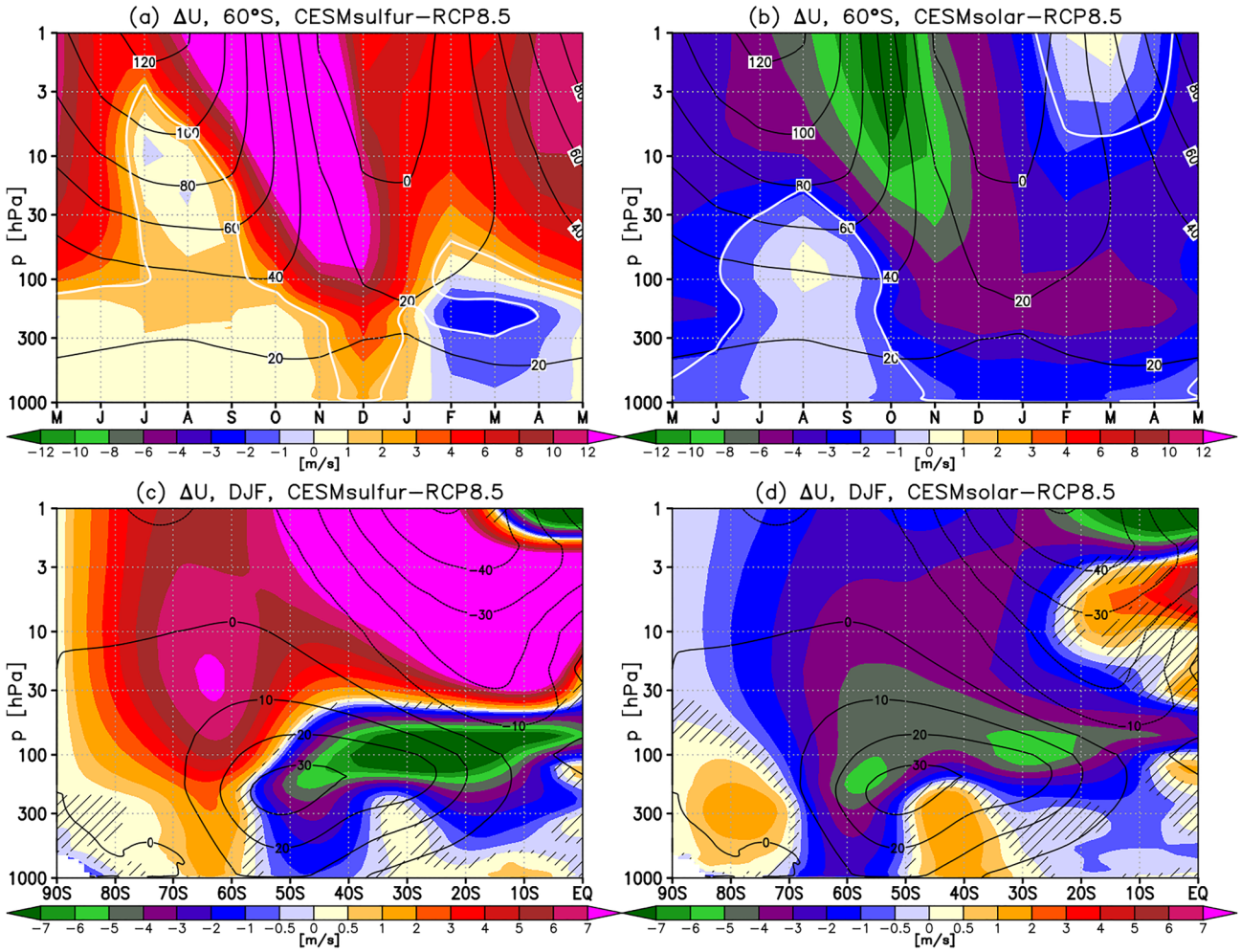

Figure 2. Stratospheric-tropospheric dynamical response to Stratospheric Aerosol Injection and solar dimming. Shading: Monthly mean differences in zonal wind (ms^{-1}) at 60°S (a, b) and December-to-February mean (DJF) mean differences in zonal wind (ms^{-1}) (c, d), averaged over 2070–2089, between CESMsulfur and RCP8.5 (a, c), and between CESMsolar and RCP8.5 (b, d). Thick white line in top panels marks the regions where the response is statistically significant (±2 standard errors). Hatching in the bottom panels indicates regions where the difference is not statistically significant (±2 standard errors). Black contours in all panels show the corresponding RCP8.5 climatology for reference.

focus here primarily on changes in the shortwave heating rates as these are directly influenced by the changes in the incoming solar radiation and aerosol loading; this is unlike the longwave heating rates which also reflect any indirect changes in atmospheric circulation and/or the temperatures themselves. In contrast to the stratospheric warming simulated in CESMsulfur, the reduction in solar constant in CESMsolar decreases absorption of shortwave radiation by stratospheric ozone and the resulting heating, thereby leading to a small cooling in the mid- and upper stratosphere. The magnitude of the upper stratospheric heating rate and temperature perturbation is comparable to that associated with variation induced by the 11-year solar cycle (e.g., Bednarz et al., 2019), although the spectral distribution of the anomalous solar forcing differs between the two cases.

Changes in stratospheric heating rates have important consequences for stratospheric circulation during dynamically active seasons (autumn to spring in each hemisphere). The aerosol absorption in CESMsulfur increases horizontal gradients of shortwave heating rates and temperature. Since atmospheric temperatures and winds are closely related via the thermal wind balance, this strengthens the stratospheric jets in each hemisphere (Figures 2 and S3 in Supporting Information S1). Such strengthening of the stratospheric jets has now been recognized as an important part of the atmospheric response to SAI (e.g., Richter et al., 2017; Simpson et al., 2019; Visioni et al., 2020; Banerjee et al., 2021), which would otherwise not be reproduced by the reduction in the solar

constant itself (Ferraro et al., 2015; Visioni, MacMartin, & Kravitz, 2021). In late austral spring, the SH westerly response likely corresponds to delayed break-up of the polar vortex (Figure 2a.)

However, what has not been acknowledged before is that the reduction in the solar constant also induces a dynamical response in the stratosphere, in particular the weakening of the stratospheric jets simulated in both hemispheres (Figures 2 and S4 in Supporting Information S1). In late austral spring, this likely corresponds to the accelerated break-up of the polar vortex. The SH easterly response is related to the anomalous propagation and breaking of planetary waves in the stratosphere (Figure S5 in Supporting Information S1), here likely as the result of the tropospheric cooling, whereas this effect is dampened by the aerosol-induced lower stratospheric heating in CESMsulfur (Figure S6 in Supporting Information S1). Furthermore, the reduction in stratospheric heating under solar dimming also contributes to the dynamical response by weakening the meridional gradients of short-wave heating rates and temperature in the upper stratosphere from autumn to spring. Interactions of the zonal mean flow with planetary waves further amplify the anomalous easterly flow and facilitate its propagation from the upper stratosphere to the troposphere (Figure 2b), where it modulates surface climate variability. While the top-down influence of the stratosphere on the troposphere under solar dimming cannot be decoupled in our runs from those related to the in-situ changes in the tropical tropospheric temperatures, the clear downward propagation of the stratospheric signal to the troposphere provides evidence for the importance of the top-down effect. Additional idealized studies would be needed to quantify the relative importance of the different processes. Here, we mainly highlight the existence of the stratospheric dynamical response under solar dimming and point out the first-order impact it has on the SH near-surface climate (see below). We note that a similar weakening of the SH polar vortex under solar dimming is also found when the response is compared against the present-day conditions (Figure S8 in Supporting Information S1). In that case, however, the interpretation of the causes of the response is confounded by the long-term recovery of stratospheric ozone (not shown) and its contribution to the short-wave heating rate changes (Figure S7b in Supporting Information S1), as well as by a small overcooling simulated in the tropical troposphere (Figure S7d in Supporting Information S1).

4. Tropospheric Response to Solar Dimming versus SAI

We focus the subsequent discussion on the Southern Hemisphere, where the development and propagation of the stratospheric circulation responses in the two geoengineering experiments (Figure 2) result in contrastingly different tropospheric responses during austral summer (Figure 3). In particular, Figure 3a shows the response of the near-surface eddy-driven jet (EDJ), which plays an important role in determining the location of storm tracks and other midlatitude weather patterns (e.g., Trenberth, 1991), and of the Southern Annular Mode (SAM; Thompson & Wallace, 2000), a dominant mode of variability in the SH and a manifestation of vertical coupling in the atmosphere. In CESMsulfur, the strengthening of the stratospheric zonal winds propagates down to the troposphere, resulting in a poleward shift of the EDJ by ∼1° (Figure 3a). This is commensurate with a tendency toward an increased sea level pressure difference between the mid- and high latitudes (i.e., a positive SAM phase). In stark contrast, the weakening of the SH stratospheric zonal winds under solar dimming in CESMsolar results in an equatorward shift of EDJ of ∼2° and a weakening of the sea level pressure difference (i.e., a negative SAM phase).

Changes in the position of the midlatitude jets are tightly correlated with shifts in the tropical Hadley Circulation (HC; Kang & Polvani, 2011; Waugh et al., 2018). Consistently, we find that the equatorward shift of the EDJ in CESMsolar is commensurate with an equatorward shift of the southern edge of the HC (Figure 3a). The magnitude of this HC shift is approximately half of that of the midlatitude jet shift, in agreement with the relationship inferred from the observational record (Kang & Polvani, 2011). In contrast, the poleward shift of the EDJ in CESMsulfur is commensurate with a small poleward shift of the HC edge. Changes in the position of HC edges in turn are associated with distinct changes in hydrological patterns (Polvani et al., 2011; Scheff & Frierson, 2012; Schmidt & Grise, 2017; Waugh et al., 2018). In CESMsolar, there is a significant equatorward shift in the position of the SH subtropical dry zone, which is not reproduced in the SAI simulations. Regarding changes in precipitation itself, the two experiments simulate significantly different zonal mean precipitation responses over large parts of the SH (Figure 3b).

We note that changes in the EDJ, HC and the associated impacts on the hydrological cycle have also been associated with changes in the horizontal temperature gradients within the troposphere (Adam et al., 2014). In

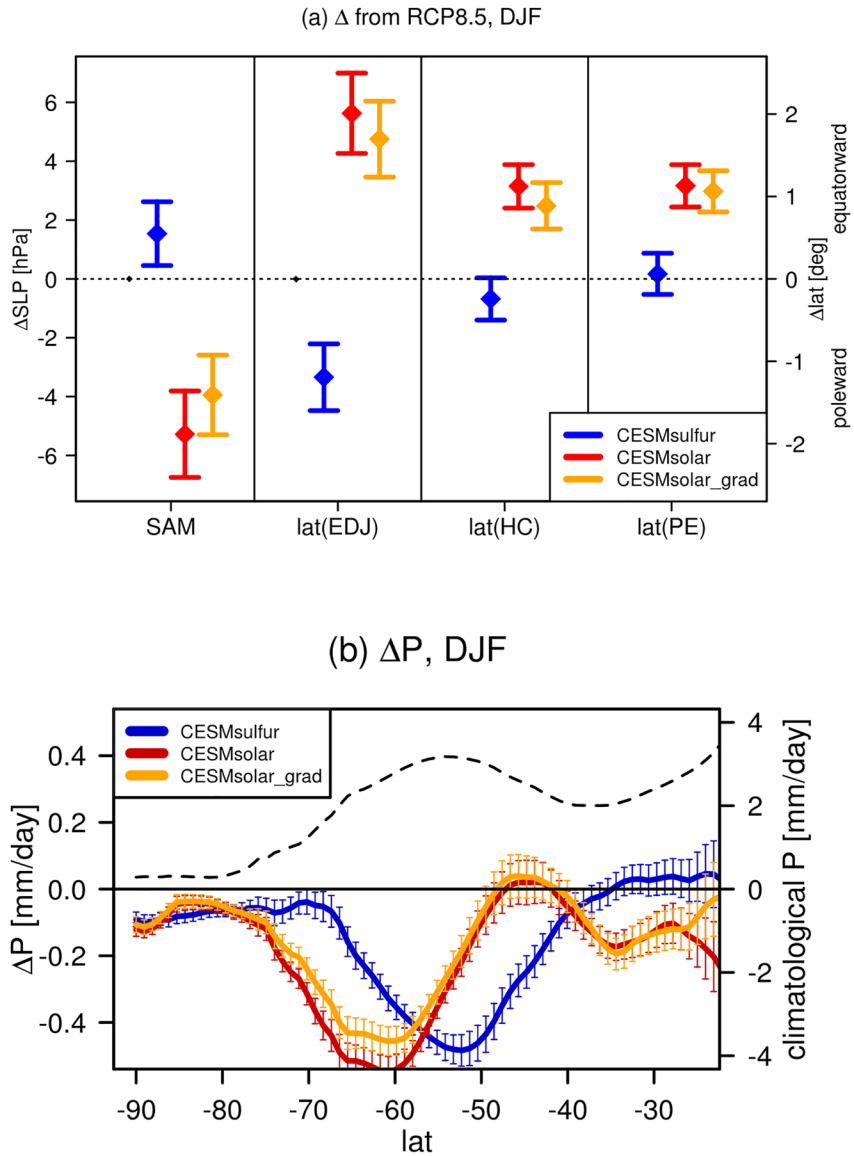

Figure 3. Impacts on the Southern Hemisphere (SH) tropospheric climate. (a) The DJF differences between 2,070 and 2,089 mean Southern Annular Mode index (see Section 2), and the location of the SH eddy-driven jet, the edge of the SH Hadley Cell and the edge of the SH subtropical dry zone (PE) between each of the CESMsulfur (blue), CESMsolar (red), CESMsolar_grad (orange) experiments and RCP8.5. Whiskers indicate ±2 standard errors of the difference in means. (b) The DJF differences in precipitation (mm/day) between 2,070 and 2,089 CESMsulfur (blue), CESMsolar (red), CESMsolar_grad (orange) experiments and RCP8.5. The dashed black line (with scale on the right hand side) indicates climatological mean precipitation in RCP8.5 for reference. The analogous figure, but for the differences compared against BASE (i.e., 2,011–2,030 mean of RCP8.5) is shown in Figure S11 in Supporting Information S1.

order to rule out the dominant role of these to the SH surface climate response simulated in our solar dimming experiments, we analyze an analogous experiment (here denoted CESMsolar_grad; Visioni, MacMartin, & Kravitz, 2021) where the reduction in solar constant was applied in a latitudinally varying manner so as to minimize changes in inter-hemispheric and equator-to-pole surface temperature gradients. The resulting changes in the SAM index, the location of the SH mid-latitude jet, the edge of the HC, and the subtropical dry zone in CESMsolar_grad were found to be qualitatively and quantitatively similar to the experiments with the uniform reduction in solar constant, CESMsolar (Figure 3a). This implies that changes in the horizontal surface temperature gradients are unlikely to be the primary driver of the SH tropospheric climate responses simulated in our solar dimming runs. We note that some statistically significant differences in the precipitation responses are

nonetheless present between the two solar dimming simulations (Figure 3b), illustrating that the role of horizontal surface temperature gradients cannot be neglected.

5. Verification in a Multi-Model Framework

We have demonstrated above that the reduction in the incoming solar radiation in CESM and the associated changes in tropospheric and stratospheric temperatures induce a dynamical response in the stratosphere that propagates down to the troposphere during the austral summer, thereby leading to coherent changes in the SH surface climate that contrast strongly with the analogous tropospheric signatures of SAI. We have established a chain of evidence and proposed a mechanism, and now we verify that our single-model results apply also to other models. We use the multi-model simulations carried out as part of GeoMIP (Kravitz et al., 2015), whereby the surface temperature increase from rising GHGs following the SSP5-85 scenario (Meinshausen et al., 2020) is offset to reach temperatures under the intermediate SSP2-4.5 scenario by means of either sulfate aerosol injection in the equatorial region (G6sulfur) or by a reduction in the solar constant (G6solar). While the magnitude of the global warming that is offset by geoengineering differs between our CESM and the GeoMIP simulations (over 5°C by the end of the century in CESM, vs. 2°C on average in the G6 models in the same period), the experimental protocols are overall similar, thereby allowing for a qualitative comparison between the two responses.

Figure 4 shows changes in the modified SAM index, and the positions of the SH midlatitude jet, Hadley Cell (HC) edge, and the subtropical dry zone edge during austral summer under geoengineering in G6sulfur and G6solar relative to SSP5-8.5, as simulated by the participating models. We clearly see that the sulfate injections in G6sulfur largely cancel the SSP5-8.5 response, or leave small residuals in the SH climate response, across the models (blue bars, Figure 4). In stark contrast, solar dimming in G6solar leaves changes in the SH climate which are much larger in magnitude (red bars, Figure 4). The G6solar responses also show a much better agreement in the sign of the changes across the models: with the exception of the CNRM model, all of the models simulate a weakening of the SH upper stratospheric jet in austral spring in G6solar, which then propagates down to the troposphere in the austral summer (Figures S9 and S10 in Supporting Information S1). In the troposphere, this top-down response leads to a distinct weakening of the pressure difference between the mid- and high southern latitudes, an equatorward shift of the SH mid-latitude jet, HC edge, and the subtropical dry zone (Figure 4). The above multi-model results are qualitatively similar to those simulated in our CESM experiments, and thus demonstrate the validity of our conclusions in a wider multi-model context.

We note that the six models differ considerably with regard to their chemistry and microphysics (e.g., only CESM, UKESM, and CNRM include interactive stratospheric ozone chemistry). In the case of the one model that does not reproduce our results (CNRM), the imposed reduction in the incoming solar radiation was somewhat lower than for the other models (1.4% in CNRM compared to 2.0% averaged across the six models, see Visioni, MacMartin, Kravitz, et al., 2021), which could have impacted the simulated dynamical response.

6. Discussion

We have demonstrated that reducing the solar constant in climate models alters the tropospheric and stratospheric heating rates and temperatures and, thus, induces a stratospheric dynamical response that propagates from the upper stratosphere down to the troposphere. While the importance of stratospheric dynamical variability has been previously overlooked in the solar dimming context, we have showed that this process can exert a first-order influence on some of the changes in the SH surface climate diagnosed from the solar-dimming experiments, thereby allowing for an erroneous attribution of the simulated tropospheric signatures to the impacts of geoengineering using sulfate aerosol injection. Future assessments of SAI using solar dimming simulations as a simpler analogue should take this effect fully into consideration when evaluating the simulated surface impacts of geoengineering.

Our results can also be applied to paleoclimate studies which try to understand the climate of previous epochs when the sun was fainter, and their parallels with the present-day climate change. Goldblatt et al. (2021) suggested the importance of changes in low cloud coverage based on vertical stability and thermodynamic arguments in the Faint Young Sun problem, where in the Archean period onwards glaciations were sparse even though the sun was fainter. We suggest that changes in the tropospheric circulation brought about by a dynamical response from the stratosphere could be another contributing factor to the cloud cover changes that would merit further

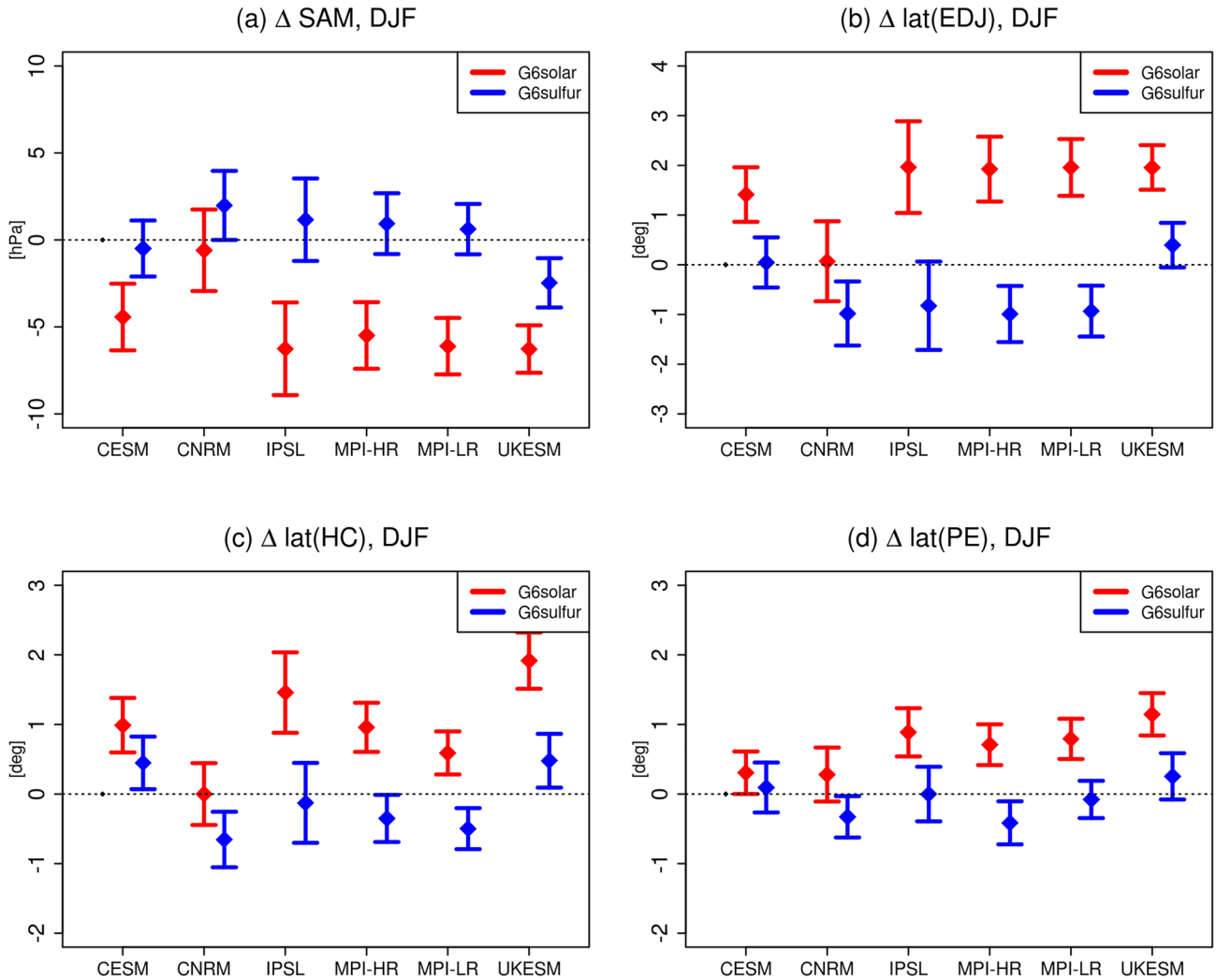

Figure 4. Verification of the impacts on the Southern Hemisphere (SH) tropospheric climate in a multi-model framework. The December-to-February mean (DJF) differences between 2080–2099 mean (a) Southern Annular Mode index (see Section 2), (b) the location of the SH eddy-driven jet, (c) the location of the edge of the SH Hadley Cell and (d) the location of the edge of the SH subtropical dry zone (PE) between each of the GeoMIP G6sulfur (blue) and GeoMIP G6solar (red) experiments and SSP5-8.5. Results are calculated separately for each model. Whiskers indicate ±2 standard errors of the difference in means. The analogous figure, but for the differences compared against the present-day reference period are shown in Figure S12 in Supporting Information S1.

investigation; this is particularly underscored if considering solar reduction of up to 20% in the paleoclimate studies, as compared to the reduction of a few percent in our simulations.

Finally, our results further demonstrate the importance of considering the stratosphere, as well as the troposphere, as an active contributor to the SH near-surface climate change. Numerous studies showed the crucial role of the springtime temperature anomalies in the Antarctic lower stratosphere brought about by Antarctic ozone depletion and its later recovery for driving the recent trends in the SH mid- and high latitude surface climate (e.g., Son et al., 2009; Polvani et al., 2011; McLandress et al., 2011; Banerjee et al., 2020). Here, we have demonstrated the importance of stratospheric dynamical variability in the geoengineering context, not only for solar dimming as an analogue for SAI-type experiments but also for proposed space-based sun-shading methods.

Appendix A: Metrics of the SH Tropospheric Climate Change

We use four metrics of the Southern Hemisphere (SH) tropospheric climate change. The modified Southern Annular Mode (SAM) index is defined here as the difference between zonal mean sea level pressure at 50°S and 70°S. The definition is similar to the commonly used station-based SAM index that uses the 40°S and 65°S

latitudes (Gong & Wang, 1999); the different latitudes chosen here correspond to those where the magnitude of the sea level pressure response to geoengineering simulated in Community Earth System Model (CESM) is largest (not shown).

The metrics for the location of the SH eddy-driven jet (EDJ), edge of the Hadley Circulation (HC), and of the subtropical dry zone are defined following Waugh et al. (2018). In particular, the location of EDJ is defined as the location of the maximum of zonal mean zonal wind at 850 hPa, here assumed to be the center of the grid containing the maximum value. The location of the edge of HC is defined as the latitude where the meridional stream function at 500 hPa poleward of the tropical minimum changes sign. If more zero-crossing latitudes are found within 20° of the initial one, the value of the metric is set to missing data for that year. The location of the edge of the subtropical dry zone is defined as the latitude where the difference between model precipitation and evaporation changes sign poleward from the subtropical minimum but equatorward from 70°S. If there are more zero-crossing latitudes, the metric is set to missing data for that year. The location of the HC edge and the subtropical dry zone edge is approximated to lie midway between the centers of the adjacent grids containing the positive and negative values.

Conflict of Interest

The authors declare no conflicts of interest relevant to this study.

Data Availability Statement

The GeoMIP G6 data are available from https://esgf-node.llnl.gov/search/cmip6/. CESMsulfur and CESM RCP8.5 data are available from https://doi.org/10.5065/D6JH3JXX. CESMsolar and CESMsolar_grad data are available from https://doi.org/10.7298/b9ws-jj47 and https://doi.org/10.7298/z8c9-3p43.

Acknowledgments
We would like to acknowledge high-performance computing support from Cheyenne (https://doi.org/10.5065/D6RX99HX) provided by NCAR's Computational and Information Systems Laboratory, sponsored by the National Science Foundation. The authors thank Simone Tilmes for performing the GLENS model simulations. Support was provided by the Atkinson Center for Sustainability at Cornell University for EMB, DV, and DGM; and by the National Science Foundation through agreement CBET-1818759 for DV and DGM. Support for BK was provided in part by the National Science Foundation through agreement CBET-1931641, the Indiana University Environmental Resilience Institute, and the Prepared for Environmental Change Grand Challenge initiative.

References

Adam, O., Schneider, T., & Harnik, N. (2014). Role of changes in mean temperatures versus temperature gradients in the recent widening of the Hadley circulation. *Journal of Climate*, *27*(19), 7450–7461.

Banerjee, A., Butler, A. H., Polvani, L. M., Robock, A., Simpson, I. R., & Sun, L. (2021). Robust winter warming over Eurasia under stratospheric sulfate geoengineering—The role of stratospheric dynamics. *Atmospheric Chemistry and Physics*, *21*, 6985–6997. https://doi.org/10.5194/acp-21-6985-2021

Banerjee, A., Fyfe, J. C., Polvani, L. M., Waugh, D., & Chang, K. L. (2020). A pause in Southern Hemisphere circulation trends due to the Montreal Protocol. *Nature*, *579*, 544–548. https://doi.org/10.1038/s41586-020-2120-4

Bednarz, E. M., Maycock, A. C., Telford, P. J., Braesicke, P., Abraham, N. L., & Pyle, J. A. (2019). Simulating the atmospheric response to the 11-year solar cycle forcing with the UM-UKCA model: The role of detection method and natural variability. *Atmospheric Chemistry and Physics*, *19*, 5209–5233. https://doi.org/10.5194/acp-19-5209-2019

Crutzen, P. J. (2006). Albedo enhancement by stratospheric sulfur injections: A contribution to resolve a policy dilemma? *Climatic Change*, *77*, 211. https://doi.org/10.1007/s10584-006-9101-y

Eyring, V., Bony, S., Meehl, G. A., Senior, C. A., Stevens, B., Stouffer, R. J., & Taylor, K. E. (2016). Overview of the coupled model intercomparison project phase 6 (CMIP6) experimental design and organization. *Geoscientific Model Development*, *9*, 1937–1958. https://doi.org/10.5194/gmd-9-1937-2016

Ferraro, A. J., Charlton-Perez, A. J., & Highwood, E. J. (2015). Stratospheric dynamics and midlatitude jets under geoengineering with space mirrors and sulfate and titania aerosols. *Journal of Geophysical Research: Atmospheres*, *120*(2), 414–429.

Goldblatt, C., McDonald, V. L., & McCusker, K. E. (2021). Earth's long-term climate stabilized by clouds. *Nature Geoscience*, *14*, 143–150. https://doi.org/10.1038/s41561-021-00691-7

Gong, D., & Wang, S. (1999). Definition of Antarctic oscillation index. *Geophysical Research Letters*, *26*, 459–462. https://doi.org/10.1029/1999gl900003

Govindasamy, B., & Caldeira, K. (2000). Geoengineering Earth's radiation balance to mitigate CO_2-induced climate change. *Geophysical Research Letters*, *27*(14), 2141–2144. https://doi.org/10.1029/1999GL006086

Gray, L. J., Beer, J., Geller, M., Haigh, J. D., Lockwood, M., Matthes, K., et al. (2010). Solar influences on climate. *Reviews of Geophysics*, *48*, 53. https://doi.org/10.1029/2009rg000282

Kalidindi, S., Bala, G., Modak, A., & Caldeira, K. (2015). Modeling of solar radiation management: A comparison of simulations using reduced solar constant and stratospheric sulphate aerosols. *Climate Dynamics*, *44*(9), 2909–2925. https://doi.org/10.1007/s00382-014-2240-3

Kang, S. M., & Polvani, L. M. (2011). The interannual relationship between the latitude of the eddy-driven jet and the edge of the Hadley cell. *Journal of Climate*, *24*(2), 563–568.

Kodera, K., & Kuroda, Y. (2002). Dynamical response to the solar cycle. *Journal of Geophysical Research: Atmospheres*, *107*, 12. https://doi.org/10.1029/2002jd002224

Kravitz, B., Caldeira, K., Boucher, O., Robock, A., Rasch, P. J., Alterskjær, K., et al. (2013). Climate model response from the Geoengineering Model Intercomparison Project (GeoMIP). *Journal of Geophysical Research: Atmospheres*, *118*(15), 8320–8332. https://doi.org/10.1002/jgrd.50646

Kravitz, B., MacMartin, D. G., Tilmes, S., Richter, J. H., Mills, M. J., Cheng, W., et al. (2019). Comparing surface and stratospheric impacts of geoengineering with different SO_2 injection strategies. *Journal of Geophysical Research: Atmospheres*, *124*(14), 7900–7918.

Kravitz, B., Robock, A., Tilmes, S., Boucher, O., English, J. M., Irvine, P. J., et al. (2015). The Geoengineering Model Intercomparison Project Phase 6 (GeoMIP6): Simulation design and preliminary results. *Geoscientific Model Development*, *8*, 3379–3392. https://doi.org/10.5194/gmd-8-3379-2015

McCusker, K. E., Battisti, D. S., & Bitz, C. M. (2015). Inability of stratospheric sulfate aerosol injections to preserve the West Antarctic Ice Sheet. *Geophysical Research Letters*, *42*(12), 4989–4997.

McLandress, C., Shepherd, T. G., Scinocca, J. F., Plummer, D. A., Sigmond, M., Jonsson, A. I., & Reader, M. C. (2011). Separating the dynamical effects of climate change and ozone depletion. Part II: Southern hemisphere troposphere. *Journal of Climate*, *24*(6), 1850–1868.

Meinshausen, M., Nicholls, Z. R. J., Lewis, J., Gidden, M. J., Vogel, E., Freund, M., et al. (2020). The shared socio-economic pathway (SSP) greenhouse gas concentrations and their extensions to 2,500. *Geoscientific Model Development*, *13*, 3571–3605. https://doi.org/10.5194/gmd-13-3571-2020

Mills, M. J., Richter, J. H., Tilmes, S., Kravitz, B., Macmartin, D. G., Glanville, A. A., et al. (2017). Radiative and chemical response to interactive stratospheric sulfate aerosols in fully coupled CESM1(WACCM). *Journal of Geophysical Research: Atmospheres*, *122*(23), 13061–13078. https://doi.org/10.1002/2017JD027006

National Academies of Sciences, Engineering, and Medicine (NASEM). (2021). *Reflecting sunlight: Recommendations for solar geoengineering research and research governance*. The National Academies Press. https://doi.org/10.17226/25762

Polvani, L. M., Waugh, D. W., Correa, G. J. P., & Son, S.-W. (2011). Stratospheric ozone depletion: The main driver of twentieth century atmospheric circulation changes in the Southern Hemisphere? *Journal of Climate*, *24*, 210–227. https://doi.org/10.1175/2010jcli3772.1

Richter, J. H., Tilmes, S., Mills, M. J., Tribbia, J. J., Kravitz, B., Macmartin, D. G., et al. (2017). Stratospheric dynamical response and ozone feedbacks in the presence of SO_2 injections. *Journal of Geophysical Research: Atmospheres*, *122*(23), 12557–12573. https://doi.org/10.1002/2017JD026912

Scheff, J., & Frierson, D. M. W. (2012). Robust future precipitation declines in CMIP5 largely reflect the poleward expansion of model subtropical dry zones. *Geophysical Research Letters*, *39*, L18704. https://doi.org/10.1029/2012gl052910

Schmidt, D. F., & Grise, K. M. (2017). The response of local precipitation and sea level pressure to Hadley cell expansion. *Geophysical Research Letters*, *44*, 10573–10582. https://doi.org/10.1002/2017gl075380

Simpson, I., Tilmes, S., Richter, J., Kravitz, B., MacMartin, D., Mills, M., et al. (2019). The regional hydroclimate response to stratospheric sulfate geoengineering and the role of stratospheric heating. *Journal of Geophysical Research: Atmospheres*, *214*, 12587–12616. https://doi.org/10.1029/2019jd031093

Son, S. W., Tandon, N. F., Polvani, L. M., & Waugh, D. W. (2009). Ozone hole and Southern Hemisphere climate change. *Geophysical Research Letters*, *36*(5), L15705. https://doi.org/10.1029/2009gl038671

Thompson, D. W. J., & Wallace, J. M. (2000). Annular modes in the extratropical circulation. Part I: Month-to-month variability. *Journal of Climate*, *13*(5), 1000–1016. https://doi.org/10.1175/1520-0442(2000)01360;1000:amitec62;2.0.co;2

Tilmes, S., Müller, R., & Salawitch, R. (2008). The sensitivity of polar ozone depletion to proposed geoengineering schemes. *Science*, *320*, 1201–1204. https://doi.org/10.1126/science.1153966

Tilmes, S., Richter, J. H., Kravitz, B., MacMartin, D. G., Mills, M. J., Simpson, I. R., et al. (2018). CESM1(WACCM) stratospheric aerosol geoengineering large ensemble project. *Bulletin America Meteorology Social*, *99*, 2361–2371. https://doi.org/10.1175/BAMS-D-17-0267.1

Trenberth, K. E. (1991). Storm tracks in the Southern Hemisphere. *Journal of the Atmospheric Sciences*, *48*(19), 2159–2178.

Visioni, D., MacMartin, D. G., & Kravitz, B. (2021). Is turning down the sun a good proxy for stratospheric sulfate geoengineering? *Journal of Geophysical Research: Atmospheres*, *126*, e2020JD033952. https://doi.org/10.1029/2020JD033952

Visioni, D., MacMartin, D. G., Kravitz, B., Boucher, O., Jones, A., Lurton, T., et al. (2021). Identifying the sources of uncertainty in climate model simulations of solar radiation modification with the G6sulfur and G6solar Geoengineering Model Intercomparison Project (GeoMIP) simulations. *Atmospheric Chemistry and Physics*, *21*, 10039–10063. https://doi.org/10.5194/acp-21-10039-2021

Visioni, D., MacMartin, D. G., Kravitz, B., Lee, W., Simpson, I. R., & Richter, J. H. (2020). Reduced poleward transport due to stratospheric heating under stratospheric aerosols geoengineering. *Geophysical Research Letters*, *47*, e2020GL089470. https://doi.org/10.1029/2020GL089470

Waugh, D. W., Grise, K. M., Seviour, W. J. M., Davis, S. M., Davis, N., Adam, O., et al. (2018). Revisiting the relationship among metrics of tropical expansion. *Journal of Climate*, *31*(18), 7565–7581.

Xia, L., Nowack, P. J., Tilmes, S., & Robock, A. (2017). Impacts of stratospheric sulfate geoengineering on tropospheric ozone. *Atmospheric Chemistry and Physics*, *17*, 11913–11928. https://doi.org/10.5194/acp-17-11913-2017